

Geometrical versus time-series representation of data in quantum control learning

M. Ostaszewski,¹ J.A. Miszczak,¹ and P. Sadowski¹

¹*Institute of Theoretical and Applied Informatics,
Polish Academy of Sciences, Baltycka 5, 44-100 Gliwice, Poland*

Recently machine learning techniques have become popular for analysing physical systems and solving problems occurring in quantum computing. In this paper we focus on using such techniques for finding the sequence of physical operations implementing the given quantum logical operation. In this context we analyse the flexibility of the data representation and compare the applicability of two machine learning approaches based on different representations of data. We demonstrate that the utilization of the geometrical structure of control pulses is sufficient for achieving high-fidelity of the implemented evolution. We also demonstrate that artificial neural networks, unlike geometrical methods, possess the generalization abilities enabling them to generate control pulses for the systems with variable strength of the disturbance. The presented results suggest that in some quantum control scenarios, geometrical data representation and processing is competitive to more complex methods.

I. INTRODUCTION

Spectacular progress made during the last few years rises hopes for the near-term construction of the devices based on the principles of quantum information processing [5, 44]. These principles can be used in metrology to develop new sensors and clocks [18], to advance the abilities for simulating materials or chemical reactions [31], to improve the security of data transmission [10], and to extend the capabilities of computing equipment [26, 47]. One of the enabling ingredients for developing quantum technologies is the physical implementation of the basic ingredients of the quantum computational process, namely quantum gates. The development of the methods for systematic driving the quantum dynamical system from an initial state to the desired state is the subject of quantum optimal control [12, 16, 23]. Advancements in this area are crucial for the real-world applications of quantum information processing.

The problem of finding the sequence of physical operations implementing the given quantum logical operation has been studied in many scenarios [19, 25, 32, 43, 50]. As the problem can be very demanding numerically, a significant research effort has been invested in creating algorithms [14, 33, 41] and developing dedicated software packages [30, 37], focused on the optimization problems arising in this area.

As the main research focus in the area of developing new methods for quantum control is on the gradient-based methods, recently the utilization of machine learning techniques has been proposed to address these types of optimization problems. In particular, in [49] a learning-based open-loop method to find robust control pulses for generating a set of universal quantum gates was proposed. In [36] a sampling-based approximate time-optimal control algorithm for a system with Hamiltonian fluctuations was discussed. The utilization of reinforcement learning in quantum control has also been proposed [13, 15, 17, 22, 40, 48]. In [8] the connection between tensor networks and machine learning in the context of optimization has been presented (see also [6, 7]). Moreover, recently it has been demonstrated that machine learning is able to perceive the parameters of quantum systems [28]. This suggests that the utilization of machine learning, especially in the form of artificial neural networks, can be beneficial for purpose of quantum control [20]. However, little attention has been devoted to the utilization of the simple machine learning techniques.

The aim of our work is to explore the possibilities of utilizing machine learning techniques in the analysis of the mapping between control pulses of an idealized system and control pulses of a system with drift. The approximation of this mapping is relevant for the understanding of the manifold of control pulses in noisy quantum systems. In [42] we suggested that recurrent neural networks can be used as a method for constructing such approximation. In this paper we scrutinize this approach in the context of classical machine learning methods. We compare recurrent neural networks with geometrical methods, and study the features and limitations of both approximation techniques. In the first approach, the pulses are treated as time-series. For harnessing this representation we use an artificial neural network designed for time-series as the corresponding method [27]. In the second approach, we treat the control pulse vectors as points in space, without assigning any meaning to the dimensions of the space. In this case, we use k-means clustering and kNN classifier as the methods based on geometrical relations [46].

In particular, there are two main observations that we support with the conducted numerical experiments.

- There exist nontrivial quantum control scenarios for which a simple, geometrical data representation and processing is competitive to more complex methods.
- Interpolation and extrapolation with respect to the quantum system parameters requires a sophisticated machine learning model.

For that purpose we define two learning tasks based on one underlying quantum control problem. These tasks allow us to highlight the similarities and differences in the studied methods

We focus on the problem of controlling the closed quantum system [11]. Our goal is to learn the type of the disturbance in the system and subsequently to utilize this knowledge for generating control pulses for the system with the same kind of disturbance but acting with a different strength. We achieve this by encoding the information about the turbulence (drift) present in the system using the machine learning methods and exploiting their generalization abilities.

Finally, in this work, in contrast to the common approach, we utilise random unitary matrices and because of this we probe the full space of unitary gates. The presented approach opens new possibilities for the utilization of machine learning techniques in the area of quantum control.

The rest of this paper is organized as follows. In Section II we introduce the theoretical model of the quantum system considered in our study. Section III contains the results of the numerical experiments comparing the considered machine learning approaches to quantum control pulses. We introduce two setups which are subsequently used to benchmark the efficiency of both approaches to the representation of quantum control pulses. Final remarks and conclusions are presented in Section IV. Technical details of the machine learning methods used in the paper are provided in the Appendices.

II. PRELIMINARIES – DESCRIPTION OF QUANTUM DYNAMICS

Let us consider a two-dimensional quantum system, a qubit, described by a state vector $|\psi\rangle \in \mathbb{C}^2$. The evolution of the system is described by Schrödinger equation of the form

$$\frac{d|\psi\rangle}{dt} = -iH(t)|\psi\rangle, \quad (1)$$

where H is the Hamiltonian operator, representing the energy of the system. In our model, the Hamiltonian H is a sum of two terms

$$H(t) = H_c(t) + H_\gamma, \quad (2)$$

corresponding to the *control field* and the *drift* interaction, respectively. The control Hamiltonian H_c

$$H_c(t) = h_x(t)X + h_z(t)Z, \quad (3)$$

with $X = \begin{pmatrix} 0 & 1 \\ 1 & 0 \end{pmatrix}$, $Z = \begin{pmatrix} 1 & 0 \\ 0 & -1 \end{pmatrix}$, represents the external fields used to alter the dynamics of the system.

On the other hand, the drift Hamiltonian $H_\gamma = \gamma Y$, where γ is a real parameter and $Y = iXZ$, represents the intrinsic dynamics of the system which is independent of the external interactions. Parameter γ describes the strength of this dynamics and is treated as a disturbance in our physical model.

To steer the system, one needs to choose the coefficients in Eq. (3), *ie.* $h(t) = (h_x(t), h_z(t))$. In this model, we assume that function $h(t)$ is constant in time intervals $\Delta t_i = [t_i, t_{i+1})$, which are the elements of the equal partition of the evolution time interval $T = \bigcup_{i=0}^{n-1} \Delta t_i$. Thus, control parameters $h(t)$ will be denoted as a vector of values for time intervals. Moreover, we assume that $h(t)$ has values from the interval $[-1, 1]$. Solving Eq. (1) we obtain the equation on motion for the system

$$|\psi_T\rangle = U(h(T))|\psi\rangle, \quad (4)$$

where

$$U(h(T)) = e^{H(\Delta t_n)} \dots e^{H(\Delta t_2)} e^{H(\Delta t_1)} \quad (5)$$

is the unitary matrix governing the time-evolution of the state vector. In the following, we will skip T in the above formula, *i.e.* we will note $U(h)$. The central problem of quantum control is to choose the appropriate control pulses, h_x, h_z , given the requested resulting unitary matrix.

The figure of merit in this problem is the *fidelity distance between superoperators*, defined as [21]

$$F = 1 - F_{err}, \quad (6)$$

with

$$F_{err} = \frac{1}{2N^2} \text{Tr} [(A - B(h))^\dagger (A - B(h))], \quad (7)$$

where N is the dimension of the system in question, A is the superoperator of the fixed target operator, and $B(T)$ is the evolution superoperator of operator resulting from the numerical integration of Eq. (1) with given controls. In particular, for a target unitary operator U , its superoperator A is given by the formula

$$A = U \otimes \bar{U}, \quad (8)$$

where \bar{U} is the element-wise conjugate of U . Superoperator $B(h) = U(h) \otimes \bar{U}(h)$ is obtained from the unitary operator resulting from the integration of the Eq. (1).

III. ASSESSMENT OF MACHINE LEARNING ABILITIES

A. Formulation of the problem

We assume that we have a qubit quantum system with two control fields as described by Eq. (3). Moreover, we are given a set of unitary operators and corresponding control signals $h(t)$ that can be implemented in the physical system. In our consideration, we introduce a drift H_γ to the system – an additional constant term in the system Hamiltonian. In the presence of the drift, the control signals calculated for the system without the drift cannot be used to obtain the desired evolution. One way to fix this is to estimate the drift and then recalculate all of the control signals. The drawback of this approach is that it requires the explicit knowledge of the drift Hamiltonian.

In the proposed approach, we use a machine learning method to solve the issue without learning the drift explicitly. Namely, the analysed machine learning task is used to learn a general method to modify the signals so that they would work with the system with the drift.

B. Utilization of machine learning

In order to study the utilization of machine learning for solving the above problem, we introduce two tasks centred around the concept of quantum control and approach both of them with machine learning methods. In both tasks, we use different methods of data representation, and each task is used to build a test environment for comparing the selected methods.

Both tasks are based on the same scenario and in both cases, the goal is to counteract an unknown drift occurring in the controlled quantum system. We use machine learning (ML) algorithms to *translate* the control pulses, $h^{\gamma=0}$, calculated for the system without drift, into the control pulses counteracting the drift, $h^{\gamma>0}$. General scheme for considering both tasks is presented in Fig. 1. The ability to successfully translate between control pulses is equivalent to the ability to learn the structure of the unknown drift. Thus, the approximations based on machine learning should map control pulses $h^{\gamma=0}$, into control pulses, $\tilde{h}^{\gamma>0} \approx h^{\gamma>0}$, which should be effective for controlling the system with the unknown drift. One can note that the mapping from $h^{\gamma=0}$ to $h^{\gamma>0}$ shares the mathematical properties with the problem of statistical machine translation [35], a problem which is successfully modelled with artificial neural networks [9].

We compare the effectiveness of ML by comparing the efficiency in terms of fidelity error and the generalization abilities. By the efficiency we understand the mean fidelity error, taken over target unitary matrices, between the operators generated from $h^{\gamma>0}$ using the considered approximation and target operators.

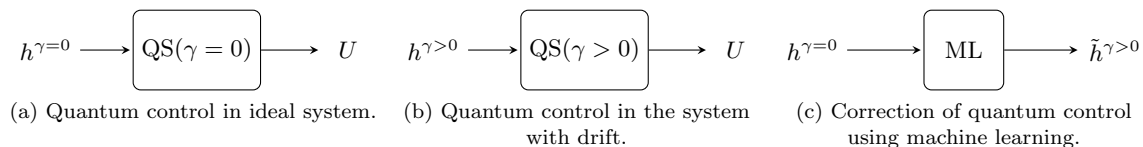


FIG. 1. Learning the structure of the drift. Here $h^{\gamma=0}$ represents control pulses implementing unitary matrix U in the quantum system QS without the drift, $h^{\gamma>0}$ respective control pulses implementing this matrix in the system with the additional drift, and $\tilde{h}^{\gamma>0}$ control pulses generated using one of the machine learning methods. Our goal is to learn the method of transforming from $h^{\gamma=0}$ to $\tilde{h}^{\gamma>0}$. This enables us to utilize the obtained ML algorithm for generating control pulses for the system with the drift, even in the situation where the strength of the drift was not available during the learning phase.

The unknown drift occurring in the studied quantum system is controlled by the strength γ . In our study, we utilize this parameter to probe ML methods. We do this by changing the way of altering this parameter in both tasks.

In the first task, our goal is to assess the efficiency of ML methods. For this reason, the drift strength is fixed during the training and testing phases. ML algorithm utilizes pairs of corresponding $h^{\gamma=0}$ and $h^{\gamma>0}$ pulses to learn about the structure of the drift. During the testing phase, we check if the $\tilde{h}^{\gamma>0}$ pulses can be used to control unitary evolution with high fidelity, and check which ML methods provide best results.

In the second task, the drift strength is variable. We consider a few values of the drift strength during the training phase and an extended values set during the test phase. This enables us, apart from testing the efficiency, to test the generalization abilities of the considered methods.

One should note that control pulses $h^{\gamma=0}$ can be seen as vectors of pairs, with the first dimension corresponding to the time slot $\{t_0, \dots, t_{n-1}\}$, and the second dimension corresponding to the values of control fields $\{h_x, h_z\}$,

$$h_{i,j}^{\gamma=0} = h_j(t_i), \quad (9)$$

with $i \in \{0, \dots, n-1\}$, $j \in \{x, z\}$. Hence, it is equally natural to treat these pulses as geometrical objects, as well as time-series. In this first case, the natural machine learning method is given by the algorithms analysing the distance between vectors, whilst if we want to harness the time-series structure it is natural to employ artificial neural networks.

C. Task I: Efficiency with constant drift

In the first task, we deal with constant drift strength. Our goal is to check the efficiency of machine learning measured by the fidelity between the unitary matrix implemented using and $h^{\gamma>0}$, and the unitary matrix obtained by using pulses $\tilde{h}^{\gamma>0}$, generated using machine learning. The considered scenario is presented in Fig. 2.

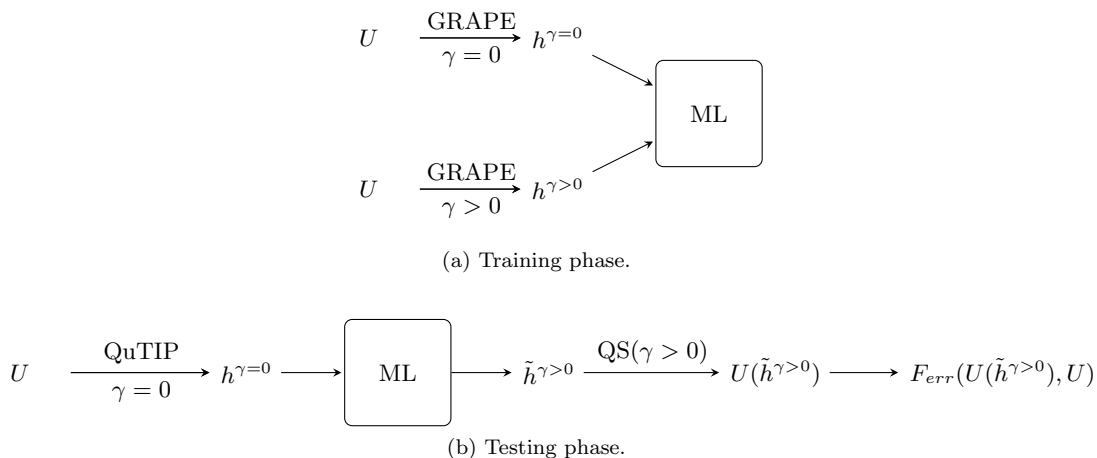


FIG. 2. Task I: Assessment of the machine learning efficiency. We assume that we need to implement unitary matrix U by controlling Quantum System (QS). (a) Training phase. We use QuTIP package to generate control pulses $h^{\gamma=0}$ and $h^{\gamma>0}$ for $\gamma = 0$ and $\gamma > 0$ respectively. In the training phase, pairs $(h^{\gamma=0}, h^{\gamma>0})$ are used to train the machine learning algorithm. (b) Testing phase. In the testing phase, machine learning algorithm is used to translate $h^{\gamma=0}$ into control pulses $\tilde{h}^{\gamma>0}$ which implements target unitary matrix U_k on a quantum system with undesired drift, $QS(\gamma > 0)$.

The procedure describing numerical experiments executed in the scope of Task I consists of the following steps.

- 1. Generating training set** Generate samples of Haar random unitary matrices [38, 39], U_k , and using GRAPE algorithm implemented in QuTIP [1, 29, 30], generate $(h^{\gamma=0}, h^{\gamma>0})$ pairs corresponding to U_k and fixed $\gamma > 0$.

In the presented numerical experiments, GRAPE algorithm is always initialized by identity matrix and the exact implementation of sampling random Haar unitary matrices is available at [3]. All numerical experiments are performed for evolution time $T = 2.1$, divided into sixteen intervals $n = 16$. The range of values of the parameter γ is restricted to the interval $[0, 1]$. This is due to the fact that it is adjusted to the restrictions for the parameters of the physical model. One should note that we were not able to find satisfactory control pulses for higher values of γ using the gradient-based method.

- 2. Training** To create correction scheme (see Fig. 1(c)) we perform the following steps.

- (a) **Train artificial neural network** Utilize $h^{\gamma=0}$ as an input and treat the corresponding $h^{\gamma>0}$ as an output reference. As a loss function, we utilize mean squared error between target $h^{\gamma>0}$, and prediction of artificial neural network $\tilde{h}^{\gamma>0}$. The input of the LSTM is a pair $x_t = (h_x^{\gamma=0}(t), h_z^{\gamma=0}(t))$ (see Appendix A).
- (b) **Train the clustering correction algorithm** Using training pairs $(h^{\gamma=0}, h^{\gamma>0})$ compute corrections, called correction control pulses, $\Delta h = h^{\gamma>0} - h^{\gamma=0}$. Next, evaluate k -means algorithm on the Δh . Finally, compute average correction control pulse \tilde{C}_j , for each cluster resulting from k -means algorithm, where j is an index of a cluster. Detailed description of the clustering correction algorithm is provided in Appendix B 1. It is important to note that by clustering Δh pulses, we obtain natural clusters on $h^{\gamma=0}$ pulses. Therefore, we can execute kNN algorithm on test $h^{\gamma=0}$ and the training set to determine the correction, which is equivalent to finding the desired $\tilde{h}^{\gamma>0}$. The kNN algorithm has number of neighbours set to $k = 4$.

3. **Testing** The procedure consists of the following steps (see Fig. 2(b)).

- (a) Generate Haar random unitary matrices U_k .
- (b) Use GRAPE to generate a testing set consisting of $h^{\gamma=0}$ for U_k .
- (c) Use the trained ML algorithm to generate $\tilde{h}^{\gamma>0}$ for each $h^{\gamma=0}$ in the testing set.
- (d) Use $\tilde{h}^{\gamma>0}$ to construct operator $U(\tilde{h}^{\gamma>0})$ assuming the drift $\gamma > 0$.
- (e) Use $h^{\gamma=0}$ to construct operator $U(h^{\gamma=0})$ from testing $h^{\gamma=0}$, also assuming the drift $\gamma > 0$. This provides a reference point, *ie.* the difference between $F_{err}(U_k, U(h^{\gamma=0}))$ and $F_{err}(U_k, U(\tilde{h}^{\gamma>0}))$, reflecting the quality of the correction $\tilde{h}^{\gamma>0}$ of $h^{\gamma=0}$.

It should be noted that the algorithms used in the numerical experiments directly work on $(h^{\gamma=0}, h^{\gamma>0})$ pairs. However, the evaluation of the efficiency requires the comparison on the level of operators corresponding to the considered control pulses. Therefore, $(h^{\gamma=0}, U_k)$ pairs are used in the testing data. The efficiency is calculated as the *mean fidelity* over the set of unitary matrices U_k ,

$$\frac{1}{M} \sum_{k=1}^M (1 - F_{err}(U_k, U(h_k))), \quad (10)$$

where h_k are control pulses corresponding to unitary matrix U_k and M is the number of unitary matrices. For the sake of clarity, we do not use the indexing of the control pulses if the relation between them and the unitary matrix can be deduced from the context.

We can distinguish two reference values for which the efficiency of the considered approximation is compared, namely

- (R1) the mean fidelity between operators obtained from $h^{\gamma=0}$, applied on a system with drift and target operators, obtained in the last step of testing,
- (R2) one *ie.* the maximal value which can be obtained from fidelity function.

It is reasonable to obtain the efficiency higher than the value from point (R1), which represents the situation of not using any correction at all. However, the closer the efficiency of the methods to the value from point (R2), the higher its effectiveness in the described scenario.

1. Efficiency of LSTM

As it has already been mentioned, the sequence of control pulses can be naturally represented as a time series. This type of data is in many cases analysed using a specialised type of artificial neural networks, namely Long Short-Term Memory (LSTM) neural networks, developed harnessing time-series character of the data. Thus, we can use LSTM as the approximation function translating the correction scheme for control pulses. The trained artificial neural network will be used as a map from $h^{\gamma=0}$ to $\tilde{h}^{\gamma>0}$.

In numerical experiments executed to assess the efficiency of LSTM, we generate 5000 random unitary matrices and train the neural network to predict $h^{\gamma>0}$ based on $h^{\gamma=0}$. For each value of gamma, a new artificial neural network is trained. The network is given the reference $(h^{\gamma=0}, h^{\gamma>0})$ pairs as a training set. For each γ value, the following results were obtained with LSTM networks trained on 3000 control pulses. The tests were performed on the set of 2000 control pulses.

As one can see in Table I, the results obtained by the GRAPE algorithm are better than those obtained from LSTM network. This effect is caused by the fact that the artificial neural network utilizes the data generated from gradient-based method as target data. However, the results presented in Table I demonstrate that LSTM network can achieve efficiency with errors of the same order of magnitude as the reference data. Moreover, one should note that for higher values of gamma parameter the data obtained from GRAPE contain many outliers, *ie.* there is a significant number of matrices for which the resulting fidelity is below the acceptable level of 0.90.

2. Efficiency of clustering

The second ML method we use is based on the purely geometrical representation of the data. To exploit the geometrical representation of the control pulses, we use k -means algorithm to utilize mean control from the cluster to correct $h^{\gamma=0}$. From the computational point of view, the advantage of this method is its simplicity. One should also note that the geometrical representation does not assign any order to the coordinates of the pulses and relies on the distance between vectors only.

As the input data, we take 3000 random unitary matrices and generate corresponding $h^{\gamma>0}$, $h^{\gamma=0}$ and Δh vectors. Here our goal is to check if the resulting clustering provides efficient correction. To this end, for each cluster, we calculate mean correction and apply it to $h^{\gamma=0}$ from respective clusters. Next, we calculate the mean fidelity for operators obtained from $\tilde{h}^{\gamma>0}$ signals and compare it with the efficiency of $h^{\gamma>0}$ and the efficiency of $h^{\gamma=0}$ applied on the system with undesired drift. Moreover, we repeat this method on the approximations of Δh presented in section B 2.

As one can see in Fig. 3, for each kind of approximation method, there exists k such that applying the correction scheme, being mean Δh within corresponding cluster, is better than the mean fidelity of application of $h^{\gamma=0}$ with $\gamma \neq 0$. Moreover, the clustering on the raw data, without any kind of approximation, yields significantly better results in comparison to approximation variants. This demonstrates that the methods used for approximation are not suitable for reducing the dimensionality in this case.

In Fig. 4 one can see the important characteristics of the algorithm, namely its insensitivity to the number of samples in the training set. One can see that the clustering with a fixed parameter k gives similar results for training sets consisting of 1000 and 5000 samples. The obtained results suggest that clustering can be used to achieve high fidelity of the control pulses even for the situation where only a small number of examples is used.

The last part of the assessment procedure consists of the efficiency test of the whole correction scheme, *ie.* we aim at answering what is the efficiency when we use kNN classifier (see Sec. B 3). In this case the efficiency of kNN should be limited by the efficiency resulting from clustering. As we can see in Fig. 5, kNN classifier has similar results on the test set as the clustering on the training set.

3. Comparison of the efficiency

The main conclusion one can draw from the obtained results is that the clustering methods can achieve surprisingly good efficiency in the considered task. One can see in Fig. 5 that for the number of clusters close to 300, we obtain the efficiency similar to LSTM.

This behaviour suggests that the quantum control pulses have a geometrical structure which can be captured and harnessed using k -means and kNN algorithms. The results obtained using this approach are very similar to the results obtained using a significantly more complicated approach represented by LSTM. This suggests that for the considered task, the utilization of artificial neural networks is not the only machine learning method which should be considered.

Method	γ			
	0.2	0.4	0.6	0.8
$\tilde{h}^{\gamma>0}$ from LSTM	.994	.991	.982	.951
$h^{\gamma>0}$ from GRAPE	.999	.999	.998	.989
$h^{\gamma=0}$ from GRAPE	.903	.657	.372	.165

TABLE I. Comparison of efficiency (mean fidelity) for $H_\gamma = \gamma Y$ for different methods of obtaining control pulses. Time of the evolution was set to $T = 2.1$. We restricted the magnitude of control pulses to interval $[-1, 1]$. The number of time slots was set to $n = 16$. Fidelity obtained using the artificial neural network ($\tilde{h}^{\gamma>0}$) is very similar to the efficiency obtained using gradient method. As expected, fidelity obtained using the original pulses ($h^{\gamma=0}$) deteriorates with the increasing strength of the drift.

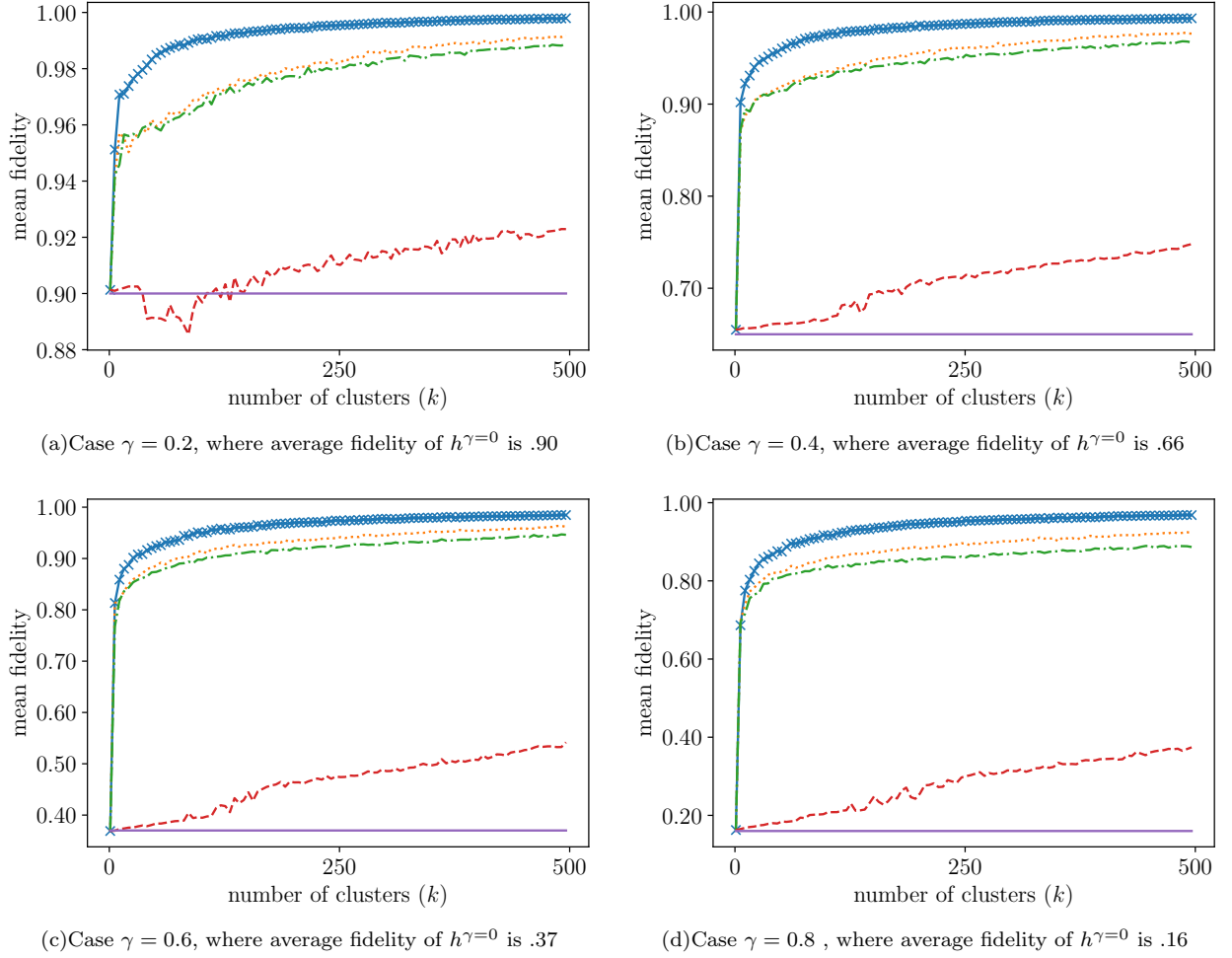


FIG. 3. The comparisons of the efficiency of corrections from clustering with the efficiency of NPC. The analysis was performed on 3000 samples. The number of clusters on axis x varies from 1 to 496 with step 5. Values marked with blue \times correspond to clustering directly on Δh . Orange dotted line corresponds to clustering on approximated data by f_{poly4} function, and dot-dash green line corresponds to clustering on approximated data by f_{poly3} (see Appendix B 2). Red dashed lines corresponds to the clustering on approximated data by combination of sinusoid. Purple continuous line corresponds to the average fidelity obtained from the application of $h^{\gamma=0}$ on the system with drift Hamiltonian.

D. Task II: Generalization with variable drift

1. Task Details

Having assessed the efficiency of the machine learning methods in the scenario where the drift strength is fixed, we now analyse their generalization abilities. To this end we introduce the second task which extends the first by allowing the manipulation of the drift strength.

One should note that, as in Task I, we assume that the drift is unknown during the learning phase. However, in contrast to the situation in Task I, now we train out algorithm using different system parameters. In other words, the algorithm is given not only the information about the pairs $(h^{\gamma=0}, h^{\gamma>0})$, but additionally each pair is associated with the drift strength. The task is to learn how to modify the control signals so that it would work for the values of γ not included in the learning examples. The idea is illustrated in Fig. 6.

During the testing phase, the trained algorithm also operates on the control pulses supplemented with the information about the target value of the drift strength. The values of parameter γ occurring in this phase can differ from the values utilized in the learning phase. This scenario is presented in Fig. 6(b).

For the purpose of analysing the ability to generalize the correction scheme we have to fix the reference values, which will be used to benchmark the generalization efficiency of the utilized methods. For our purpose we define

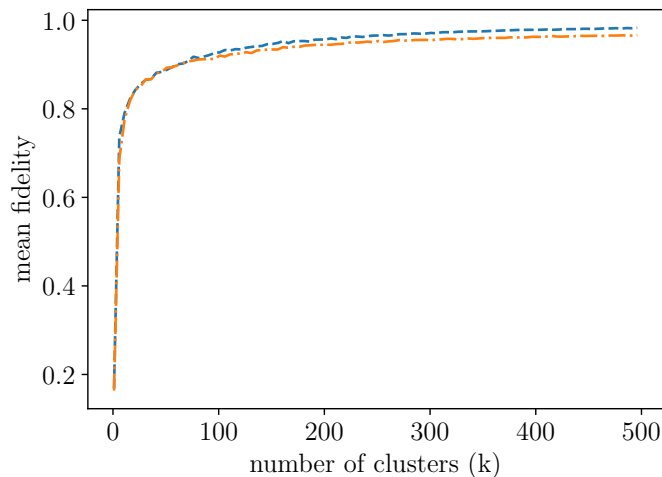


FIG. 4. Insensitivity of the clustering to the size of the training set. The graph plotted with a blue dashed line corresponds to the sample of size 1000, and the graph plotted with a orange dot-dashed line corresponds to the sample of size 5000. For number of clusters equal to 500, we saturate the abilities of the clustering. In the first case the average cluster contains 2 elements, whilst in the former it contains 10 elements. The numerical experiment was performed for $\gamma = 0.8$.

reference point of generalization as the mean fidelity obtained by the algorithm trained on data with fixed parameter γ , applied to other values of the parameter. Such defined reference point provides the minimal efficiency which should be obtained by the tested algorithm in order to consider it suitable for using it for the new values of the drift strength.

The reference points are constructed as follows. Let us suppose that we have an already trained machine learning model – artificial neural network or k -means/ k NN algorithms. This model can be applied on a test set of $h^{\gamma=0}$ to reproduce corrections schemes for a system with a fixed parameter γ . The generated pulses $h^{\gamma>0}$ can be integrated with different values of parameter γ . The fidelity of the resulting operator with the target operator provides the efficiency of the approximation. In the other words, we test how efficient is $h^{\gamma>0}$ generated for some γ when we apply it to a system with different drift strength.

The reference points for k NN and LSTM models are presented in Fig. 7. As expected from the results of Task I, LSTM has higher efficiency than k NN near the value of γ used to construct the reference point.

2. Generalization efficiency

In the numerical experiments testing the generalization efficiency the input is a vector of triples, each of the form $(h_x(t), h_z(t), \gamma)$. We denote inputs as $(h^{\gamma=0}, \bar{\gamma})$, where $\bar{\gamma}$ denotes the vector with all elements equal to γ and the appropriate dimension. The constant vector with all elements equal to γ can be interpreted as the additional third dimension in the time series. Hence, in the case of artificial neural networks it is possible to utilize similar architecture as in the case of Task I. The difference is that input time point is a triple $x_t = (h_x^{\gamma=0}(t), h_z^{\gamma=0}(t), \gamma)$ (see Appendix A).

During the training phase we utilize the values of the drift strength from some set A . Next, during the test phase, we are given other drift strength values $\gamma \notin A$. In the numerical experiments presented below we use two sets of parameters for training, $A_1 = \{0.1, 0.3, 0.5\}$ and $A_2 = \{0.5, 0.7, 0.9\}$. During the testing phase we use parameters from set $B = A_1 \cup A_2 \cup \{0.2, 0.4, 0.6, 0.8\}$.

In the case of clustering, the training and the testing phases of Task II are executed as follows.

1. **Generating training set** Generate Haar random unitary matrices. Based on them, generate $h^{\gamma=0}$ and $h^{\gamma>0}$ for $\gamma \in \{0.1, 0.3, 0.5, 0.7, 0.9\}$. For each γ value we use 3000 training samples, what gives us 9000 training samples for set A_1 and 9000 for set A_2 .
2. **Training** Create approximation of the correction scheme as in Fig. 6(a)
 - (a) For LSTM network, we first create pairs $(h^{\gamma=0}, \bar{\gamma})$, with values of $\gamma \in A_1 \cup A_2$. Next we train two LSTM networks independently, the first on the training data corresponding to set A_1 and the second on the data corresponding to set A_2 . Each input $(h^{\gamma=0}, \bar{\gamma})$ has a corresponding target $h^{\gamma>0}$. Cost function is the same as in Task I.

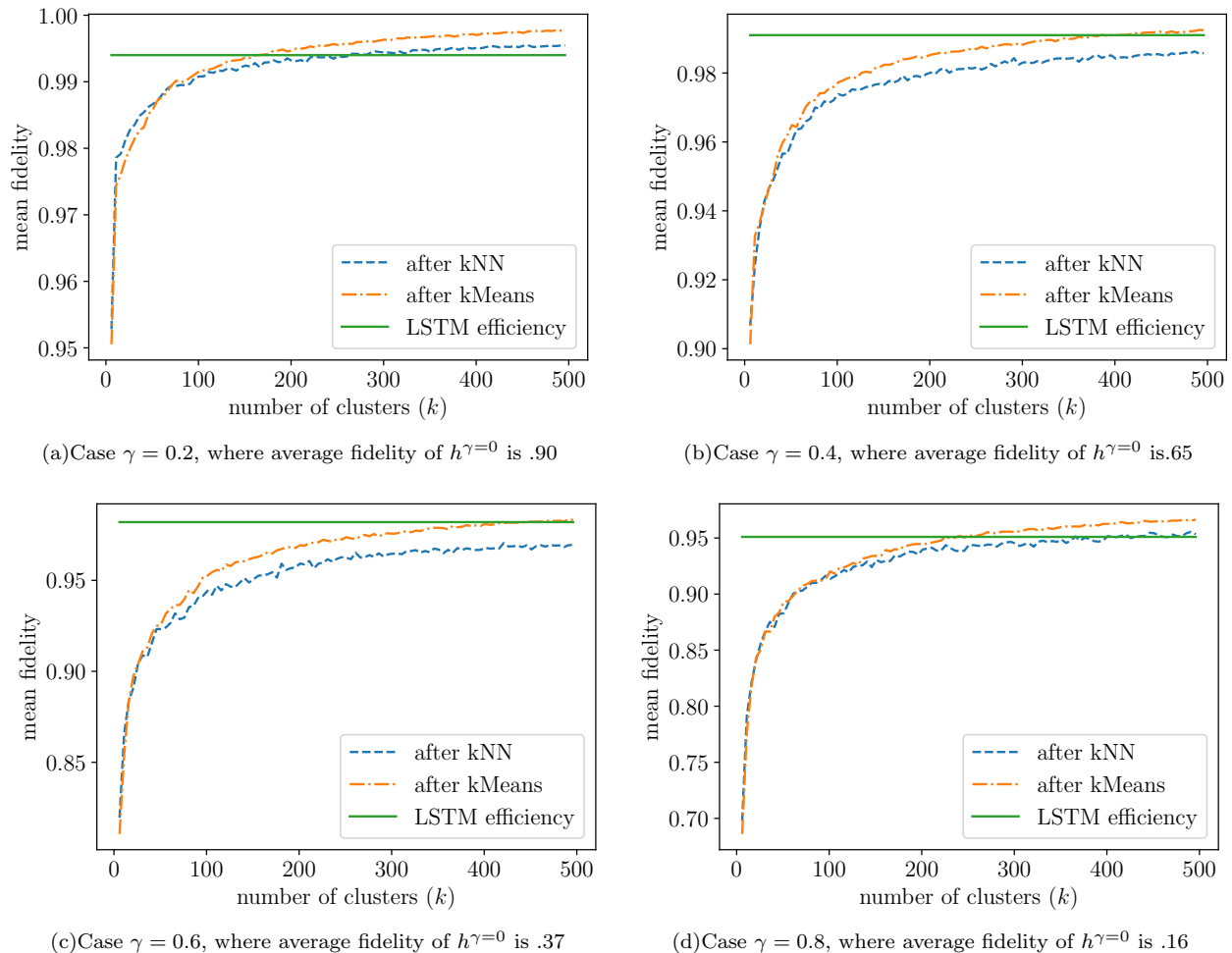


FIG. 5. The above plots show the comparisons of the efficiency of clustering on a training set (3000 samples) and classifier on a test set (2000 samples) with respect to the number of clusters, *ie.* the number of universal correction schemes. Because of low divergence, we choose one representative k in kNN algorithm *ie.* $k = 4$.

(b) For the geometrical method, first we perform the clustering algorithm with the number of clusters equal to 500, on $\Delta h = h^{\gamma>0} - h^{\gamma=0}$ obtained from $h^{\gamma>0}$ for $\gamma \in A_1$ and A_2 .

One should note that we apply the kNN on the flattened $h^{\gamma=0}$, corresponding to Δh from the clustering. However, we include additional information about the drift by adding an element equal to γ multiplied by some large number. This changes the meaning of the additional dimension and separates the vectors on the subspace spanned by the added element. In our numerical experiments, this number is equal to 1000. In kNN we choose $k = 4$.

3. Testing Generate 2000 Haar random unitary matrices and generate corresponding vectors of control pulses, $h^{\gamma=0}$. Testing phase is based on the joining $h^{\gamma=0}$ with testing value of gamma $\gamma \in B$ in a suitable manner for each algorithm. Next, using ML algorithm we generate $\tilde{h}^{\gamma>0}$, and integrate it as in Eq. (5). After that we compute the fidelity error between the obtained operator and the target operator.

One should note that each pair $(h^{\gamma=0}, \bar{\gamma})$ corresponds to a different $h^{\gamma>0}$. Hence, due to the different number of drift values used in both phases, we have different number of samples in the training and testing phases.

3. Comparison of the results

The above procedures enable us to analyse the changes in the efficiency for both methods in the function of the disturbance strength. As one can see in Fig. 8(a), the k -means/kNN has three local maxima, which correspond to

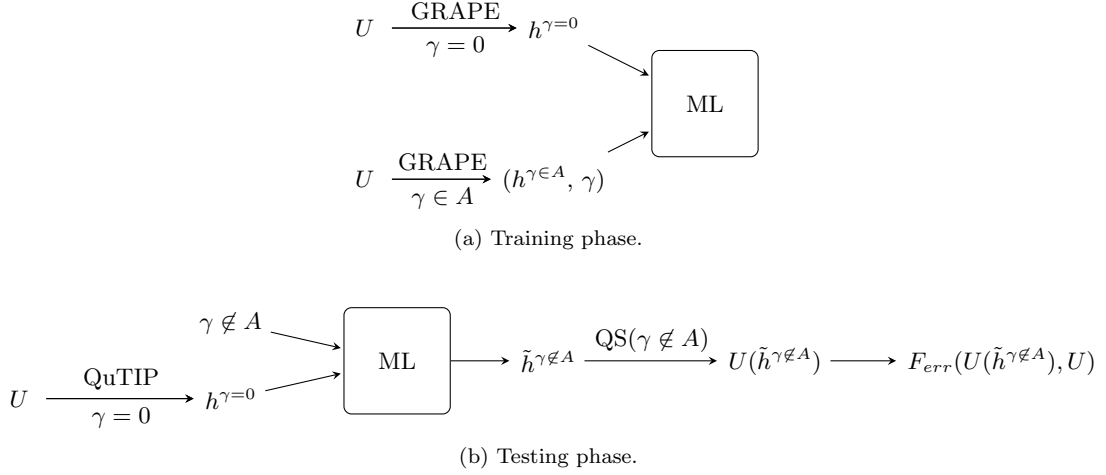


FIG. 6. Task II: Learning correction for an unknown drift. As in Task I, the goal is to implement unitary matrix U in quantum system. The difference is in the role of the γ parameter, which is not fixed during the task. (a) Training phase. We use GRAPE algorithm from the QuTIP package to generate control pulses $h^{\gamma=0}$ and $h^{\gamma \in A}$ for selected values of $\gamma \in A$. (b) Testing phase. We use trained machine learning method to translate pairs $(h^{\gamma > 0}, \gamma \notin A)$ into $\tilde{h}^{\gamma \notin A}$ for given $\gamma \in A$. Changes in the values of drift strength are used to model the changes of the internal dynamics of the system and enables the analysis of the generalization abilities.

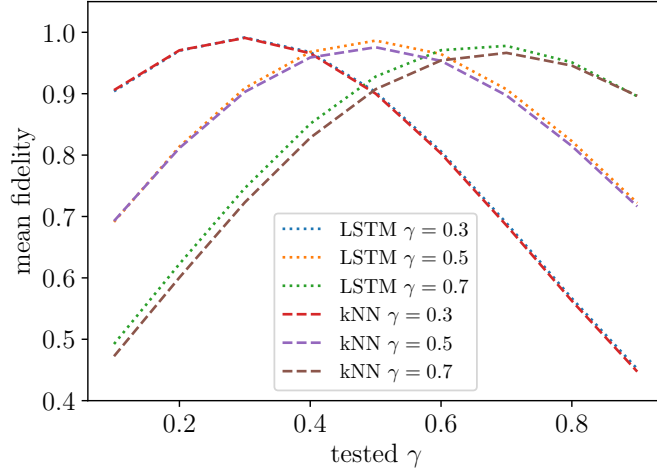


FIG. 7. Reference point of generalization for LSTM and kNN.

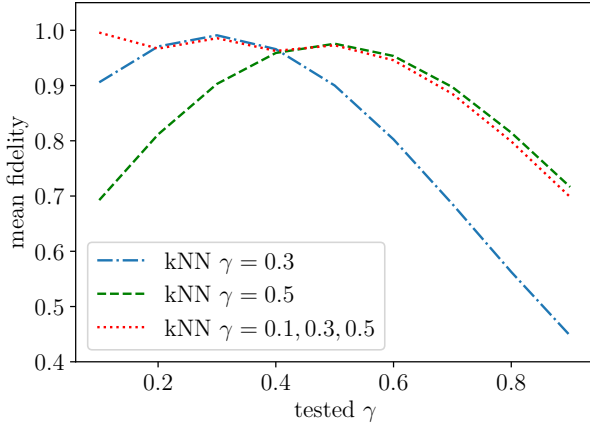
the values of drift strength on which the algorithm was trained. Therefore, this algorithm has noticeable drops in the interpolation. One can conclude that the clustering trained on the values from A is as good as the clustering trained on a single value.

Moreover, for kNN trained with $\gamma \in A_1$, the extrapolation is worse than the reference point for $\gamma = 0.5$. For kNN trained with $\gamma \in A_2$, the ability to generalize for other γ is also limited. In this case, this might be caused by the presence of outliers in the training data (see Fig 8(b)). This suggests that this method does not utilize the information about γ parameter. The additional γ in the input is not utilized and the algorithm obtains similar results as the algorithm without γ in the input.

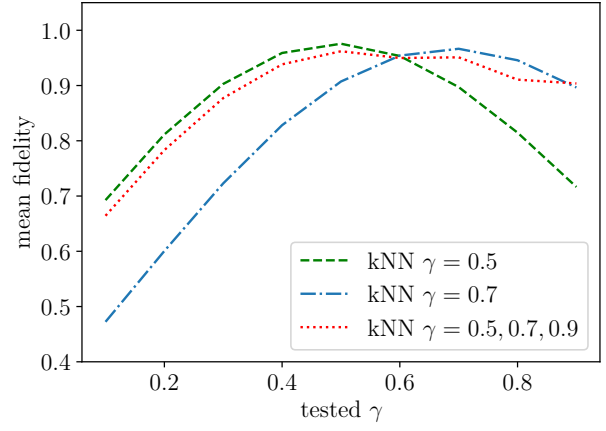
The situation is different in the case of utilizing of LSTM network, which displays the ability to generalize the correction scheme using information about parameter γ . This effect can be observed in Fig. 8(c). As one can see, LSTM has high efficiency in the neighbourhood of the training points.

Moreover, for LSTM trained with $\gamma \in A_1$, the extrapolation is better than the reference point for $\gamma = 0.5$ and especially for $\gamma = 0.3$. Thus, one can conclude that LSTM has the ability to generalize for other γ .

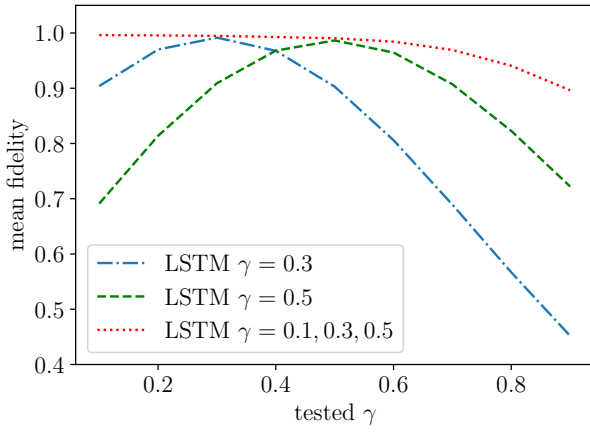
One should note that the ability of generalization does not depend on the values of γ . The efficiency of extrapo-



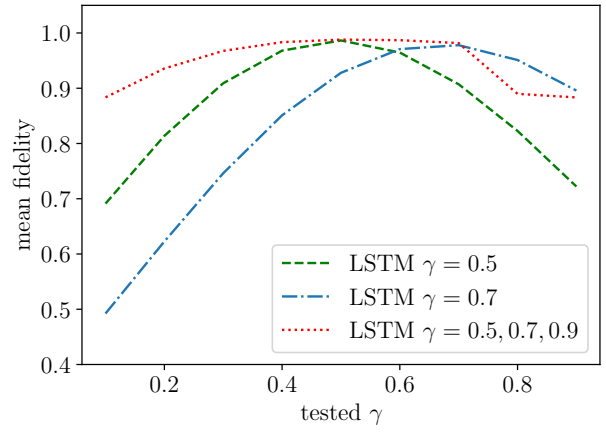
(a) Comparison of the efficiency of generalization obtained using kNN with reference points for $\gamma = 0.3$ and 0.5 .



(b) Comparison of the efficiency of generalization obtained using kNN with reference points for $\gamma = 0.5$ and 0.7 .



(c) Comparison of the efficiency of generalization obtained using LSTM with reference points for $\gamma = 0.3$ and 0.5 .



(d) Comparison of the efficiency of generalization obtained using LSTM with reference points for $\gamma = 0.5$ and 0.7 .

FIG. 8. Generalization abilities of kNN and LSTM methods. Figs. (a) and (b) represent efficiency of control pulses obtained using kNN. Figs. (c) and (d) represent efficiency of control pulses obtained using LSTM. Each plot was made for different values of drift strength used during the training phase. In all cases, the training set has size 3000, and the testing set has size 2000.

lation depends only on the difference between the testing values and the training values. LSTM method has better generalization abilities when trained with small values of γ and used to generate control pulses for large values, as well as in the case where we use larger values for training and extrapolate to smaller values.

IV. CONCLUDING REMARKS

The results presented in this paper demonstrate that both neural networks and geometrical methods provide good correction schemes and enable counteracting the undesired interaction present in the physical system. The performed numerical experiments suggest that there are some types of nontrivial quantum control tasks for which simple geometrical data representation and processing is as good as much more sophisticated machine learning models. We have also observed that the same tasks can become much more demanding when interpolating and extrapolating with respect to the system parameters is expected.

One should note that both methods studied in this work have their specific advantages and disadvantages. Numerical results suggest that recurrent neural networks have the ability to generalize their predictions with respect to the system parameters. This can be seen in the presented numerical experiments where the network trained on a limited set of gamma values also has good results for gamma values which were absent in the training process. Moreover, artificial neural networks are useful in the sense of approximation function as the trained network is a deterministic map from

$h^{\gamma=0}$ to $h^{\gamma>0}$. Because of this, one can examine a variation, continuity, and other mathematical features of this correction scheme [42].

On the other hand, the application of clustering shows that this repair scheme on its own, when generalization is not considered, can be compressed to a relatively small number of corrections. This demonstrates that the continuous process of quantum control can be represented by a relatively small number of representative control pulses. Such method has the efficiency of approximation similar as in the case of the recurrent neural networks. Results presented in this paper suggest that the machine learning approach based on simple, geometrical methods can provide a viable approach for the analysing of the locally affine transformations on the space of control pulses.

The analysis presented in this paper can be seen as a step in the process of compiling quantum operations into control pulses. Machine learning methods could be utilized to improve the quality of the obtained control pulses. This would require the application of the presented methods for quantum control methods used in current quantum computers.

ACKNOWLEDGEMENTS

MO acknowledges support from Polish National Science Center scholarship 2018/28/T/ST6/00429. JAM acknowledges support from Polish National Science Center grant 2014/15/B/ST6/05204. Authors would like to thank Daniel Burgarth and Leonardo Banchi for discussions about quantum control, Adam Glos, Bartosz Grabowski, and Wojciech Masarczyk for discussions concerning the details of LSTM architecture, and Izabela Mischczak for reviewing the manuscript. Numerical calculations were possible thanks to the support of PL-Grid Infrastructure.

-
- [1] QuTiP - Quantum Toolbox in Python, 2012-.
 - [2] Tensorflow: An open-source machine learning framework for everyone, 2016-.
 - [3] Approximation of quantum control using lstm, 2018-. https://github.com/ZKSI/qcontrol_lstm_approx.
 - [4] Ma. Abadi, P. Barham, J. Chen, Z. Chen, A. Davis, J. Dean, M. Devin, S. Ghemawat, G. Irving, M. Isard, M. Kudlur, J. Levenberg, R. Monga, S. Moore, D.G. Murray, B. Steiner, P. Tucker, V. Vasudevan, P. Warden, M. Wicke, Y. Yu, and X. Zheng. TensorFlow: A system for large-scale machine learning. In *12th USENIX Symposium on Operating Systems Design and Implementation*, volume 16, pages 265–283, 2016.
 - [5] Antonio Acín, Immanuel Bloch, Harry Buhrman, Tommaso Calarco, Christopher Eichler, Jens Eisert, Daniel Esteve, Nicolas Gisin, Steffen J Glaser, Fedor Jelezko, Stefan Kuhr, Maciej Lewenstein, Max F Riedel, Piet O Schmidt, Rob Thew, Andreas Wallraff, Ian Walmsley, and Frank K Wilhelm. The quantum technologies roadmap: a European community view. *New Journal of Physics*, 20(8):080201, 2018.
 - [6] Moritz August and José Miguel Hernández-Lobato. Taking gradients through experiments: Lstms and memory proximal policy optimization for black-box quantum control. 2018.
 - [7] Moritz August and Xiaotong Ni. Using recurrent neural networks to optimize dynamical decoupling for quantum memory. *Physical Review A*, 95(1):012335, 2017.
 - [8] Moritz M August. *Lehrstuhl für Wissenschaftliches Rechnen*. PhD thesis, Technische Universität München, 2018.
 - [9] Dzmitry Bahdanau, Kyunghyun Cho, and Yoshua Bengio. Neural machine translation by jointly learning to align and translate. 2014.
 - [10] F. Benatti, M. Fannes, R. Floreanini, and D. Petritis, editors. *Quantum Information, Computation and Cryptography. An Introductory Survey of Theory, Technology and Experiments*. Lecture Notes in Physics. Springer, 2010.
 - [11] Heinz-Peter Breuer, Francesco Petruccione, et al. *The theory of open quantum systems*. Oxford University Press on Demand, 2002.
 - [12] Constantin Brif, Raj Chakrabarti, and Herschel Rabitz. Control of quantum phenomena: past, present and future. *New Journal of Physics*, 12(7):075008, 2010.
 - [13] Marin Bukov, Alexandre GR Day, Dries Sels, Phillip Weinberg, Anatoli Polkovnikov, and Pankaj Mehta. Reinforcement learning in different phases of quantum control. *Physical Review X*, 8(3):031086, 2018.
 - [14] Tommaso Caneva, Tommaso Calarco, and Simone Montangero. Chopped random-basis quantum optimization. *Phys. Rev. A*, 84:022326, Aug 2011.
 - [15] Chunlin Chen, Han-Xiong Li, Daoyi Dong, Tzyh-Jong Tarn, and Jian Chu. Fidelity-Based Probabilistic Q-Learning for Control of Quantum Systems. *IEEE Transactions on Neural Networks and Learning Systems*, 25(5):920–933, 2013.
 - [16] D. d’Alessandro. *Introduction to quantum control and dynamics*. CRC Press, 2007.
 - [17] Daoyi Dong, Chunlin Chen, Hanxiong Li, and Tzyh-Jong Tarn. Quantum Reinforcement Learning. *IEEE Transactions on Systems, Man, and Cybernetics, Part B (Cybernetics)*, 38(5):1207–1220, 2008.
 - [18] C. L. Degen, F. Reinhard, and P. Cappellaro. Quantum sensing. *Reviews of Modern Physics*, 89(3):035002, 2017.
 - [19] Patrick Doria, Tommaso Calarco, and Simone Montangero. Optimal control technique for many-body quantum dynamics. *Phys. Rev. Lett.*, 106:190501, May 2011.

- [20] Vedran Dunjko and Hans J Briegel. Machine learning & artificial intelligence in the quantum domain: a review of recent progress. *Reports on Progress in Physics*, 81(7):074001, jun 2018.
- [21] F.F. Floether, P. de Fouquieres, and S.G. Schirmer. Robust quantum gates for open systems via optimal control: Markovian versus non-markovian dynamics. *New J. Phys.*, 14(7):073023, 2012.
- [22] Thomas Fösel, Petru Tighineanu, Talitha Weiss, and Florian Marquardt. Reinforcement learning with neural networks for quantum feedback. *Physical Review X*, 8(3):031084, 2018.
- [23] Steffen J. Glaser, Ugo Boscain, Tommaso Calarco, Christiane P. Koch, Walter Köckenberger, Ronnie Kosloff, Ilya Kuprov, Burkhard Luy, Sophie Schirmer, Thomas Schulte-Herbrüggen, Dominique Sugny, and Frank K. Wilhelm. Training Schrödinger’s cat: quantum optimal control. *The European Physical Journal D*, 69(12):279, 2015.
- [24] Alex Graves, Santiago Fernández, and Jürgen Schmidhuber. Bidirectional lstm networks for improved phoneme classification and recognition. In *International Conference on Artificial Neural Networks*, pages 799–804. Springer, 2005.
- [25] Rahel Heule, Christoph Bruder, Daniel Burgarth, and Vladimir M Stojanović. Local quantum control of heisenberg spin chains. *Physical Review A*, 82(5):052333, 2010.
- [26] Mika Hirvensalo. *Quantum Computing*. Natural Computing Series. Springer, 2nd edition, 2004.
- [27] S. Hochreiter and J. Schmidhuber. Long short-term memory. *Neural Computation*, 9(8):1735–1780, 1997.
- [28] Raban Iten, Tony Metger, Henrik Wilming, Lidia Del Rio, and Renato Renner. Discovering physical concepts with neural networks. *arXiv:1807.10300*, 2018.
- [29] J.R. Johansson, P.D. Nation, and F. Nori. QuTiP: An open-source python framework for the dynamics of open quantum systems. *Comput. Phys. Commun.*, 183(8):1760 – 1772, 2012.
- [30] J.R. Johansson, P.D. Nation, and F. Nori. QuTiP 2: A python framework for the dynamics of open quantum systems. *Comput. Phys. Commun.*, 184(4):1234 – 1240, 2013.
- [31] Tomi H Johnson, Stephen R Clark, and Dieter Jaksch. What is a quantum simulator? *EPJ Quantum Technology*, 1(1):10, 2014.
- [32] Navin Khaneja, Björn Heitmann, Andreas Spörl, Haidong Yuan, Thomas Schulte-Herbrüggen, and Steffen J Glaser. Shortest paths for efficient control of indirectly coupled qubits. *Physical Review A*, 75(1):012322, 2007.
- [33] Navin Khaneja, Timo Reiss, Cindie Kehlet, Thomas Schulte-Herbrüggen, and Steffen J. Glaser. Optimal control of coupled spin dynamics: design of nmr pulse sequences by gradient ascent algorithms. *Journal of Magnetic Resonance*, 172(2):296 – 305, 2005.
- [34] Diederik P Kingma and Jimmy Ba. Adam: A method for stochastic optimization. *arXiv:1412.6980*, 2014.
- [35] Philipp Koehn. *Statistical machine translation*. Cambridge University Press, Cambridge, UK, 2009.
- [36] Sen Kuang, Peng Qi, and Shuang Cong. Approximate time-optimal control of quantum ensembles based on sampling and learning. *Physics Letters, Section A: General, Atomic and Solid State Physics*, 382(28):1858–1863, 2018.
- [37] S. Machnes, U. Sander, S. J. Glaser, P. de Fouquieres, A. Gruslys, S. Schirmer, and T. Schulte-Herbrüggen. Comparing, optimizing, and benchmarking quantum-control algorithms in a unifying programming framework. *Phys. Rev. A*, 84:022305, Aug 2011.
- [38] Francesco Mezzadri. How to generate random matrices from the classical compact groups. *NOTICES of the AMS*, 54:592–604, 2007.
- [39] J.A. Miszczak. Generating and using truly random quantum states in mathematica. *Comput. Phys. Commun.*, 183(1):118–124, 2012.
- [40] Murphy Yuezhen Niu, Sergio Boixo, Vadim N Smelyanskiy, and Hartmut Neven. Universal quantum control through deep reinforcement learning. In *AIAA Scitech 2019 Forum*, page 0954, 2019.
- [41] Morzhin Oleg and Pechen Alexander. Krotov method in optimal quantum control. i. closed systems. *arXiv preprint arXiv:1809.09562*, 2018.
- [42] M. Ostaszewski, J.A. Miszczak, L. Bianchi, and P. Sadowski. Approximation of quantum control correction scheme using deep neural networks. *Quantum Information Processing*, 2018.
- [43] Lukasz Pawela and Przemysław Sadowski. Various methods of optimizing control pulses for quantum systems with decoherence. *Quantum Information Processing*, 15(5):1937–1953, May 2016.
- [44] Max F Riedel, Daniele Binosi, Rob Thew, and Tommaso Calarco. The European quantum technologies flagship programme. *Quantum Science and Technology*, 2(3):030501, 2017.
- [45] Mike Schuster and Kuldeep K Paliwal. Bidirectional recurrent neural networks. *IEEE Transactions on Signal Processing*, 45(11):2673–2681, 1997.
- [46] Gregory Shakhnarovich, Trevor Darrell, and Piotr Indyk, editors. *Nearest-Neighbor Methods in Learning and Vision Theory and Practice*. 2006.
- [47] Mathias Soeken, Thomas Haener, and Martin Roetteler. Programming quantum computers using design automation. In *Proceedings of the 2018 Design, Automation and Test in Europe Conference and Exhibition, DATE 2018*, volume 2018, pages 137–146, 2018.
- [48] S. S. Vedaie, P. Palittapongarnpim, and B. C. Sanders. Reinforcement learning for quantum metrology via quantum control. In *2018 IEEE Photonics Society Summer Topical Meeting Series (SUM)*, pages 163–164, July 2018.
- [49] Chengzhi Wu, Franco Nori, Chunlin Chen, Daoyi Dong, Bo Qi, and Ian R. Petersen. Learning robust pulses for generating universal quantum gates. *Scientific Reports*, 6(1):36090, 2016.
- [50] Ehsan Zahedinejad, Joydip Ghosh, and Barry C. Sanders. High-fidelity single-shot toffoli gate via quantum control. *Phys. Rev. Lett.*, 114:200502, May 2015.

Appendix A: LSTM as an approximation of the correction scheme

As an approximation of the correction scheme which takes into account time series structure of data, we have used bi-directional long short-term memory (biLSTM) units [27]. LSTM is a special type of artificial neural network, which processes its hidden states in recurrent (cyclic) way.

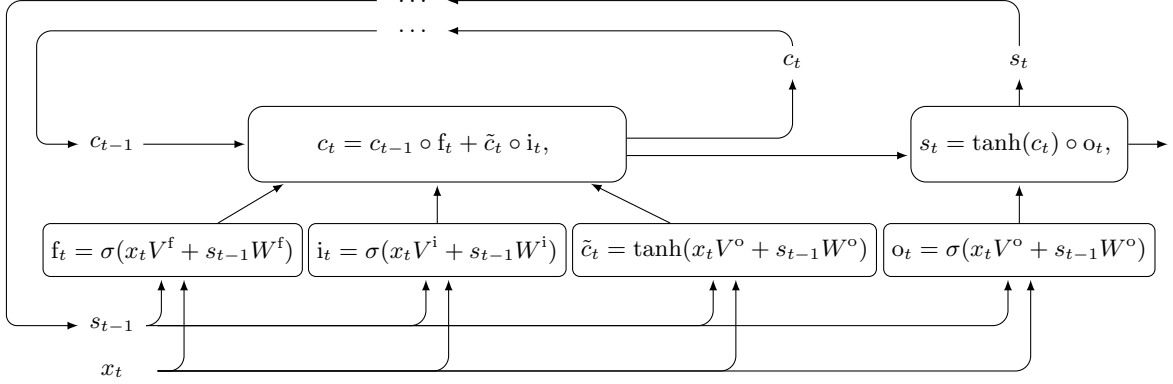


FIG. 9. Structure of LSTM network used in the numerical experiments (from [42]).

All gates have common input x_t , the current input, s_{t-1} , the previous hidden state, and the weight matrices W and V . In c_t (cell state) and s_t (hidden state), operation \circ is element-wise multiplication of two vectors. Because of sigmoid function, σ , outputs i_t , f_t and o_t of gates are vectors with elements from $[0, 1]$ interval. This construction enables the maintenance the information, which is propagated to next time step. The bi-directional version of LSTM analyses the input sequence in both directions – forwards and backwards [24, 45]. As the input, it takes $[h(t_1), h(t_2), \dots, h(t_n)]$ and $[h(t_n), h(t_{n-1}), \dots, h(t_1)]$.

The utilized architecture consists of three layers of bidirectional LSTM with the number of hidden units respectively 200, 250, and 300. The output of the last LSTM unit is merged as a element-wise sum of forward LSTM output and backward LSTM product. As the final step, the fully connected perceptron layer maps a 300-dimensional vector to the origin size. As the optimization method we used Adam optimizer [34] with learning rate 0.0001. As the cost function we chose mean squared error between the prediction of the network and the target. Numerical experiments were performed using the TensorFlow library [2, 4].

Appendix B: Function approximation by clustering method

1. Clustering correction algorithm

Algorithm 1 Clustering correction algorithm

Input: A set of affine corrections $C = \{c_i = b_i - a_i\}$, number of clusters k

1: (Optional) Approximation of Δh vectors

We choose the type of approximation (one from Eqs. (B2),(B3), or (B4)) and change the space of considered data *ie.* we express every c_i by a vector of suitable approximation coefficients – coeffs_{*i*}

2: Clustering of the set of C

Apply k -means algorithm on the set of corrections $C = \{c_i\}_i$ or on coeffs_{*i*}. As every coeffs_{*i*} corresponds to c_i , the result is the set of k clusters C_1, C_2, \dots, C_k and corresponding them labels y_i

3: Calculate output corrections as the mean correction

$$\bar{C}_i \leftarrow \frac{\sum_{c \in C_i} c}{|C_i|} \quad (\text{B1})$$

return (labels – $\{y_i\}$, corrections – $\{\bar{C}_i\}$)

Output of the above algorithm and training set of arguments gives us the approximation of the map of $h^{\gamma=0}$ to $h^{\gamma>0}$. To get correction of the new point $h^{\gamma=0}$ we need to develop a method for deciding which correction $\{\bar{C}_j\}$ should

be used. For this purpose we utilize kNN algorithm, which will be fitted on the set of training $\{h_i^{\gamma=0}\}_i$ with labels obtained during the clustering of $\{\Delta h_i\}_i$. Prediction of kNN on test $h^{\gamma=0}$ gives us the most probable cluster j , and in result the correction \tilde{C}_j which should be used to generate suitable $\tilde{h}^{\gamma>0} \approx h^{\gamma>0}$.

It should be stressed that input data in our numerical experiments are not row vectors *ie.* $h^{\gamma=0}$, $h^{\gamma>0}$ and Δh in above algorithm are matrices. Thus, for k -means and kNN algorithm, they are flattened to raw vectors.

2. Approximation schemes

In this approach, we also analyse if the data can be compressed via approximation by elementary functions

a) sinusoid

$$f_{sinusoid}(x) = \alpha_1 \sin(\alpha_2 x + \alpha_3) + \alpha_4 \sin(\alpha_5 x + \alpha_6) + \alpha_7, \quad (\text{B2})$$

with $\alpha_1 > \alpha_4$,

b) polynomial of the third degree (poly3)

$$f_{poly3}(x) = \alpha_1 x^3 + \alpha_2 x^2 + \alpha_3 x + \alpha_4, \quad (\text{B3})$$

c) polynomial of the fourth degree (poly4)

$$f_{poly4}(x) = \alpha_1 x^4 + \alpha_2 x^3 + \alpha_3 x^2 + \alpha_4 x + \alpha_5. \quad (\text{B4})$$

Here all α_i are real parameters used in the approximation. In the numerical experiments, Δh will be the signal which we will try to approximate, and thus $x = \Delta h$. Clustering is made on the parameters α_i corresponding to particular Δh .

3. k nearest neighbours algorithm

Let us assume that we have a given training set $(x_1, y_1), \dots, (x_n, y_n)$, where $x_i \in \mathbb{R}^m$ are data points, and $y_i \in \{1, \dots, l\}$ are corresponding labels. The core idea of the algorithm is as follows. For each new sample x_{n+1} we take k nearest samples from the training set, and based on the majority of votes, we assign label y_{n+1} .

Algorithm 2 kNN

Input: Hyperparameter k , training data points $(x_1, y_1), \dots, (x_n, y_n)$, and test sample x .

- 1: **for** $i = 1, \dots, n$ **do**
 - 2: $d_i \leftarrow \|x_i - x\|$
 - 3: Compute multi-set of labels S corresponding to k smallest distances d_i
 - 4: **for** $j = 1, \dots, l$ **do**
 - 5: $e_j \leftarrow \frac{|S \cap \{j\}|}{k}$
 - 6: **return** $\arg \max_j e_j$
-

One should note that it is possible to construct many variants of this algorithm by changing the applied norm. In the the scope of this work, we use Euclidean norm. Moreover, it is worth to note that this method provides an example of *instance-based method*, *ie.* it does not create any generalization rules, but compares each sample to the training set.